Atomic Force Microscopy

CONTENTS

1 Introduction 1

2 Contact Mode 1

3 Investigation of samples 2
3.1 First sample 2
3.2 Second sample 4

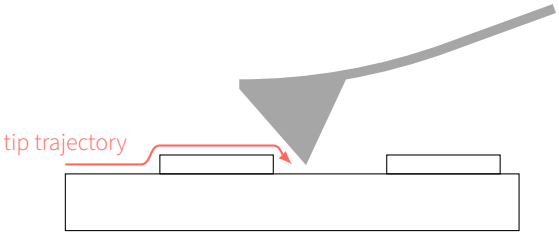

Fig. 1 | AFM contact mode. While the sample is scanned, the tip of the cantilever stays on the surface.

1 INTRODUCTION

Atomic force microscopy (AFM) continues to be at the forefront of nanoscale research, enabling groundbreaking discoveries and innovative applications across various fields. In particular, AFM stands out due to its exceptional ability to provide high-resolution imaging and to analyze both organic and inorganic samples across different environments, including ambient air, liquids, and vacuum conditions. This capability makes AFM an invaluable tool for examining the intricate architecture of nanoscale structures and investigating microscopic and submicroscopic objects that are beyond the diffraction limit of traditional optical microscopy. AFM technology has allowed scientists to achieve unprecedented resolution, facilitating detailed imaging of molecular structures and interactions. For instance, AFM has been pivotal in studying the mechanical properties and behaviors of DNA strands [1]. Moreover, the information obtained with AFM is not limited to mere topography; force spectroscopy can measure physicochemical surface properties, providing insights into adhesive forces, elasticity, and stiffness. Recent developments have advanced AFM into high-speed formats, enabling real-time observation of dynamic biological and chemical processes, which is crucial for understanding fast molecular interactions and transformations [2, 3]. Furthermore, the development of functionalized AFM tips has facilitated the mapping of chemical compositions and electrical conductivity measurements at the nanoscale, broadening its applicability to areas like materials science and nanotechnology [4, 5]. Additionally, AFM has found significant applications in the semiconductor industry for surface roughness characterization [6]. In this work we will analyze the surface two samples using AFM and Gwyddion [7], a very powerful open-source software for the processing of a very broad variety of AFM file formats. Both of the probes were scanned using the so called “contact mode”. Therefore, a short description of this techniques will be given. For more detailed information about AFM and other scanning techinques, the reader is encouraged to refer to various literature such as [8].

2 CONTACT MODE

Contact mode is a fundamental imaging technique in AFM that relies on continuous physical contact between the probe tip and the sample surface (see Fig. 1). During operation, a sharp tip at the end of a flexible cantilever interacts with the sample, with the interaction forces dominated by short-range repulsive forces arising from atomic overlap. As the tip scans across the surface, variations in surface features cause the cantilever to deflect, and these deflections are detected using a laser beam deflection system. In this system, a laser reflects off the cantilever onto a position-sensitive photodetector, which measures the deflection. To prevent damage to the sample or tip and to maintain a constant interaction force, a feedback loop adjusts the cantilever height in real time by moving the sample or the tip vertically using a piezoelectric scanner. These height adjustments are recorded to produce a topographical map of the surface with nanometer or sub-nanometer resolution. Contact mode is particularly advantageous for its high spatial resolution, simplicity of operation, and relatively fast scanning capabilities, making it suitable for imaging hard and smooth surfaces. However, the continuous tip-sample contact poses challenges, such as potential sample deformation, tip wear, and distortion due to lateral forces. Adhesion and friction forces, particularly in humid environments, can further complicate imaging and affect data accuracy. Despite these limitations, contact mode remains widely used for hard material analysis, nanofabrication processes, and topographical mapping, particularly for rigid surfaces like metals, ceramics, and crystalline structures. Its straightforward implementation and ability to resolve atomic-scale features make it a valuable tool in nanoscale

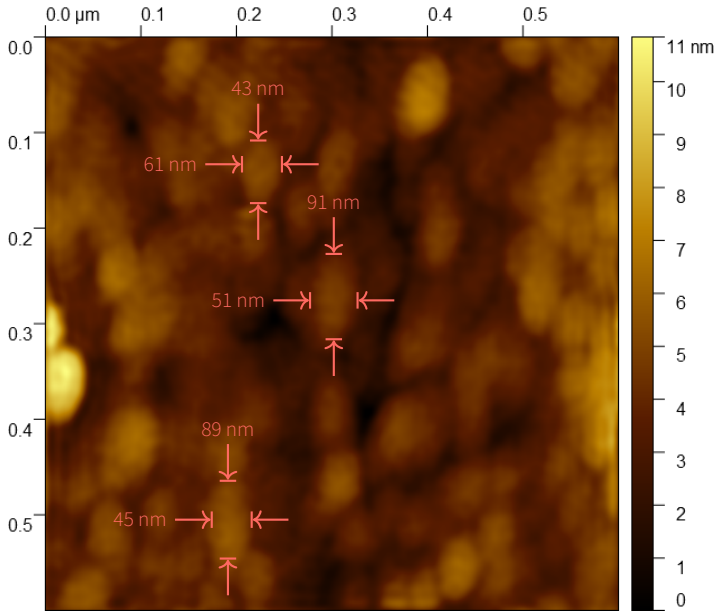

(a) The surface exhibits oval shaped elevated patterns.

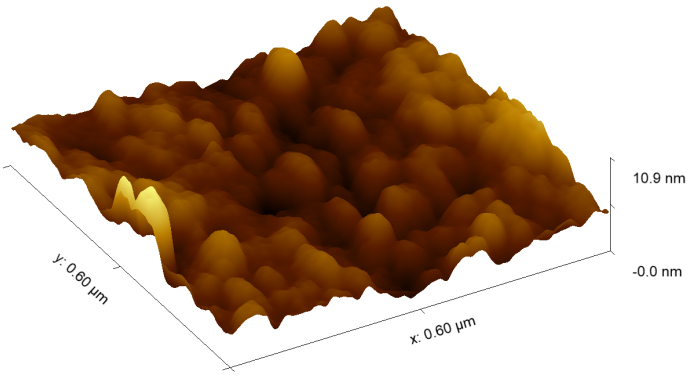

(b) 3D-plot of the surface.

Fig. 2 | AFM-image of GPU-surface after image processing techniques using Gwyddion have been applied.

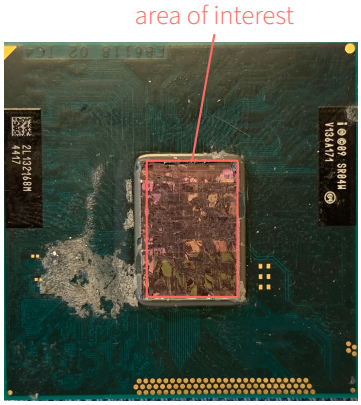

Fig. 3 | **First sample.** GPU removed from a approx. 12-year old laptop. The surface of the GPU processing unit has been forcefully scratched off.

surface characterization. For softer materials, alternative techniques like tapping mode are often preferred to minimize sample damage and mitigate issues associated with lateral forces [8, 9].

3 INVESTIGATION OF SAMPLES

3.1 FIRST SAMPLE

The first sample to be analyzed is a GPU-chip extracted from a laptop manufactured approximately 12 years ago. Upon forcefully removing the topmost layer, we exposed a shiny underlayer that is most likely composed of silicon, as depicted in Fig. 3. Given that the sample is a solid block material with no moving parts on the surface, we employed “contact mode” for the AFM imaging. This mode is advantageous for its high resolution in mapping surface topography, though it requires careful force management to avoid damaging delicate structures. Our objective is to investigate whether the AFM recordings can reveal any discernible structures that may be associated with integrated circuit (IC) logic. To begin, we captured a comprehensive overview of the surface, scanning an area of 60 µm × 60 µm. This enabled us to identify regions of interest and smoother areas that are more likely to contain the intricate features of an IC logic circuit. Subsequently, we focused on a smoother section, meticulously scanning a localized area of 600 nm × 600 nm. This decision was strategic, aiming to enhance the resolution and detail of the images, which is crucial for identifying fine structures or patterns indicative of circuit elements.

Processing the data Data analysis is done on the “height” image data using Gwyddion. Our height variations are small enough such that nonlinear effects of z-Piezo accounted for in the “height (measured)” data do not have to be considered. The following image processing techniques were applied to enhance the quality and interpretability of the AFM data:

1. *Data Process → Plane Level*: This step aims to correct any tilt in the image caused by mounting the sample not perfectly horizontal to the measurement system. The ”plane level” function computes a plane from all image points and subtracts it from the data to achieve this correction. Although the ”facet level” function is an alternative, we observed that ”plane level” provides better contrast. However, given our small scanning area of 600 nm × 600 nm, the effect of this process step is minor.

2. *Data Process → Align Rows* (Polynomial Option, Degree: 1): This technique addresses scan line defects by fitting a polynomial of degree one to each row and subtracting it, effectively removing linear slopes and yielding superior results for our data.

3. *Data Process → Correct Horizontal Scars*: This procedure targets artifacts linked to the fast scanning axis, where image stripes caused by a common scanning error (local faults in the closed loop) are prevalent. The function automatically detects and removes these scars, using adjacent lines to fill in gaps.

4. *Data Process → Basic Operations → Null Offset*: This adjustment facilitates information extraction through visual inspection by removing lateral offsets, ensuring both the x- and y-axes start at zero.

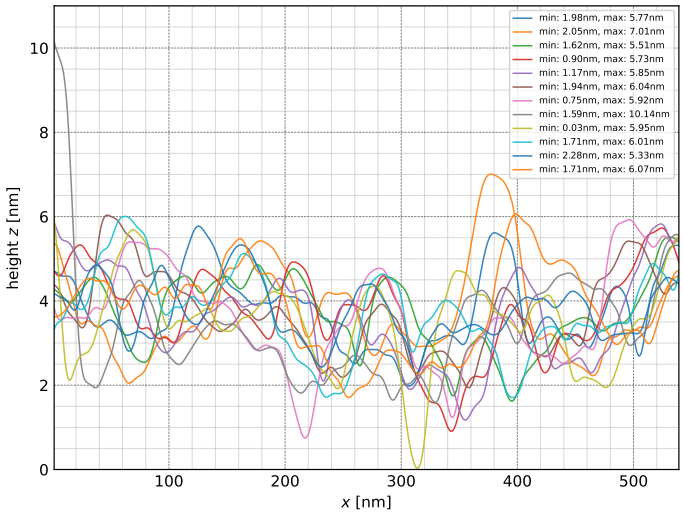

(a) Twelve roughly equidistant surface profile lines in *x*-direction.

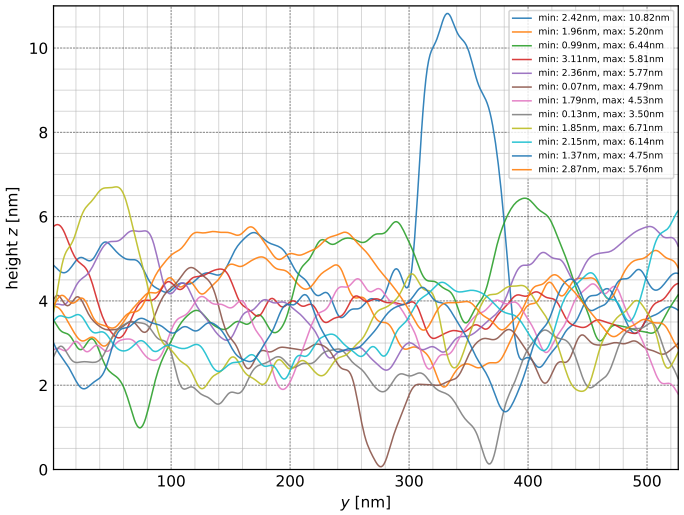

(b) Twelve roughly equidistant surface profile lines in *y*-direction.

Fig. 4 | Surface profile lines in *x*- and *y*-direction.

5. Data Process → Correct Data → 2D FFT Filtering: Fourier filtering is employed to effectively remove high-frequency artifacts resulting from ambient noise. Care was taken to avoid eliminating genuine surface features, allowing us to achieve smooth surface representation.

6. Data Process → Fix Zero: This step shifts all data points by a constant to ensure the minimum value is set to zero.

7. Tools → Stretch Color Range: This adjustment ensures that the color scale only reaches within the data's actual range, allowing for quick assessment of the height variation represented in the image, while the color map is set to "gold" for improved visualization.

The processed height data, shown in Fig. 2a, is accompanied by a 3D visualization (Fig. 2b) for improved understanding. Upon inspection, the figure reveals a granular structure characterized by oval-shaped elevations, demonstrating the effectiveness of the applied processing techniques.

Extracting dimensions To gain a clearer understanding of the dimensions of these individual oval-shaped elevations, we utilized the "measure distance" tool to determine the lateral and vertical width and of three randomly selected ovals, as depicted in Fig. 2a. We further analyzed the height profile by examining 12 approximately equidistantly selected cross-sections in both the x- and y-directions. This was accomplished using the "extract profile" tool. The resulting data is displayed in Fig. 4a and Fig. 4b. The minimum and maximum values from each profile are summarized in Tab. 1. Additionally, we calculated the mean, standard deviation, and the ratio of the standard deviation to the mean for these profiles to provide further insight into the surface characteristics.

Fast Fourier Transform When recognizing repetitive or regular patterns is challenging through visual inspection alone, a Fourier transformation can be a valuable tool. The Fourier transform breaks down an image into its sinusoidal components, highlighting periodic structures within the image. This technique is especially beneficial for identifying grid-like patterns, textures, or woven fabrics that exhibit consistent repetition. In the frequency domain, regular patterns manifest as distinctive peaks, making them easier to detect and analyze. By utilizing the Fast Fourier Transform (FFT) tool (Data Process → Correct Data → 2D FFT), and extracting the values in x- and y-direction we obtained the data shown in Fig. 5.

z-min [nm]		z-max [nm]	
in x-direction	in y-direction	in x-direction	in y-direction
1.98	2.42	5.77	10.82
2.05	1.96	7.01	5.20
1.62	0.99	5.51	6.44
0.90	3.11	5.73	5.81
1.17	2.36	5.85	5.77
1.94	0.07	6.04	4.79
0.75	1.79	5.92	4.53
1.59	0.13	10.14	3.5
0.03	1.85	5.95	6.71
1.71	2.15	6.01	6.14
2.28	1.37	5.33	4.75
1.71	2.87	6.07	5.76
		mean	
1.48	1.76	6.28	5.85
		standard deviation	
0.62	0.93	1.23	1.73
		standard deviation/mean	
0.42	0.52	0.20	0.30

Tab. 1 | Extracted data from surface profiles.

Evaluation and Discussion An IC logic structure typically comprises logic gate circuits with transistors positioned closely together. Given their fabrication processes, which generally involve a combination of deposition methods, lithography, and etching, devices of the same type, especially those in proximity, are expected to have nearly identical dimensions. Consequently, if our data captures the topography of such devices, we would anticipate minimal variance in the minimum and maximum values of the extracted height profiles. However, as shown in Table 1, the ratio of the standard deviation to the mean ranges from 20% to 52%, strongly indicating that the data likely represents a random surface profile, most probably of poly-silicon. Furthermore, a Fourier transform of the data yields graphs for x- and y-spatial frequencies that lack significant peaks, which could suggest a regular or repetitive pattern. While comparing our data with images of

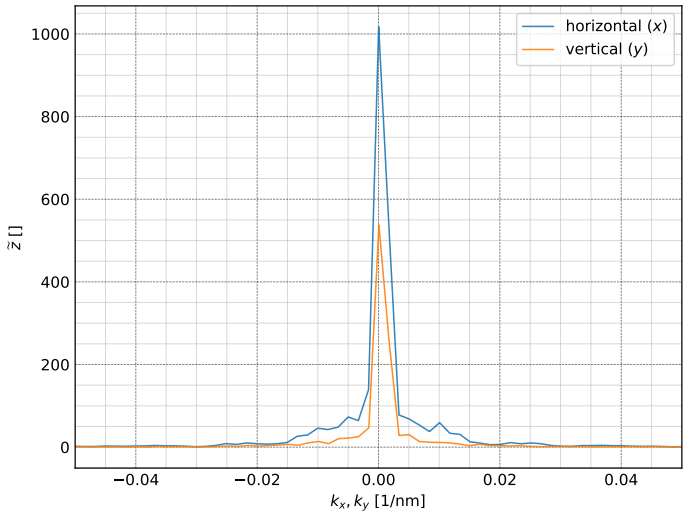

Fig. 5 | FFT-data in both x and y direction extracted from the topography depicted in Fig. 2a.

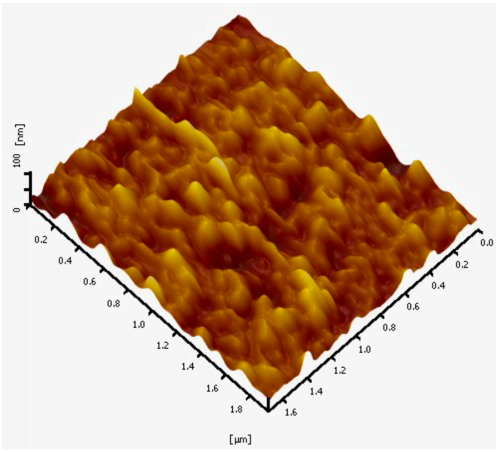

Fig. 6 | **AFM-image of a poly-silicon surface.** Taken from [11].

known IC structures could provide further insights, such images are difficult to obtain due to proprietary concerns. Nevertheless, manufacturers typically disclose the technology node of their ICs. In our case, we are dealing with 40 nm technology [10], indicating that the smallest structure dimension should be around 40 nm. It would therefore be reasonable to expect structures spanning up to a few hundred nanometers, yet no regular pattern of such dimensions is evident in our data. Conversely, an AFM image of a poly-silicon surface (Fig. 6) from [11] exhibits a strong resemblance to our data. Moreover, in other work [12] the grain size of poly-silicon was found be around 45 to 50 nm which is in very good agreement with the dimensions of the ovals observed in our data. According to an additional source [13], RMS roughness of a poly-silicon surface was reported to range between approx. 0.5 nm and 12 nm which is comparable to the values presented in Tab. 1. We think that IC logic must be hidden underneath the surface, therefore a better approach to revealing such structures would be for instance by means of nano-computed tomography (nano-CT), a high resolution 3D imaging technique.

Fig. 7 | **Second sample.** A glass substrate on which an Ag-layer has been deposited by means of thermal evaporation.

3.2 SECOND SAMPLE

The second sample under examination consists of a glass substrate with a thermally evaporated silver (Ag) layer, as depicted in Figure 7. The thickness of the Ag layer was initially measured using a profilometer. For this measurement, a portion of the surface was deliberately scratched in straight lines using a knife to create profiles that the profilometer could scan, resulting in a measured thickness of 82 nm. However, due to the limited resolution of the profilometer, this measurement has an uncertainty of approximately ±20 nm. Thus, our current goal is to utilize AFM to achieve a more precise and accurate thickness measurement. We begin by scanning a large area of 80 µm × 80 µm to locate the scratched regions on the surface. Once a descending channel-like feature is identified, we refine the scan to a smaller area of 25 µm × 25 µm, ensuring that the channel is centered. This area size provides an optimal balance, offering good resolution while maintaining a sufficient number of data points for robust arithmetic analysis. A smaller scan area might improve resolution further, but would compromise the quantity of data available for analysis.

Processing the data The analysis of the AFM-data will be done using the "height (measured)" image data as height variations in the recorded topography are sufficiently large such that the nonlinear behavior of the z-piezo must be taken into account. Utilizing Gwyddion for data analysis, we apply the following image processing techniques, facilitating our further investigation of the sample:

1. *Data Process → Align Rows* (Median Mean Option): Unlike traditional row alignment methods that adjust each line to a representative height, the Median Mean option realigns the rows so that the median of the height differences between vertically adjacent pixels becomes zero. This approach is advantageous as it better preserves significant features while being more sensitive to entirely erroneous lines. For our dataset, this option delivers the most accurate results among the available choices, clearly accentuating the step feature present in our data. We found that performing this step first lays a solid foundation for subsequent processing steps.

2. *Tools → Level data by fitting a plane through 3 points*: The tilt of the image is corrected by selecting three points that are expected to lie on the same level. Since the Ag deposition was carried out in an ultrahigh vacuum, the resulting layer is exceptionally homogeneous. As a result, this method yields highly reliable outcomes when the three points are chosen on the Ag layer (points shown as white crosses in Fig. 8a).

2. *Data Process → Fix Zero*: This step shifts all data points by a

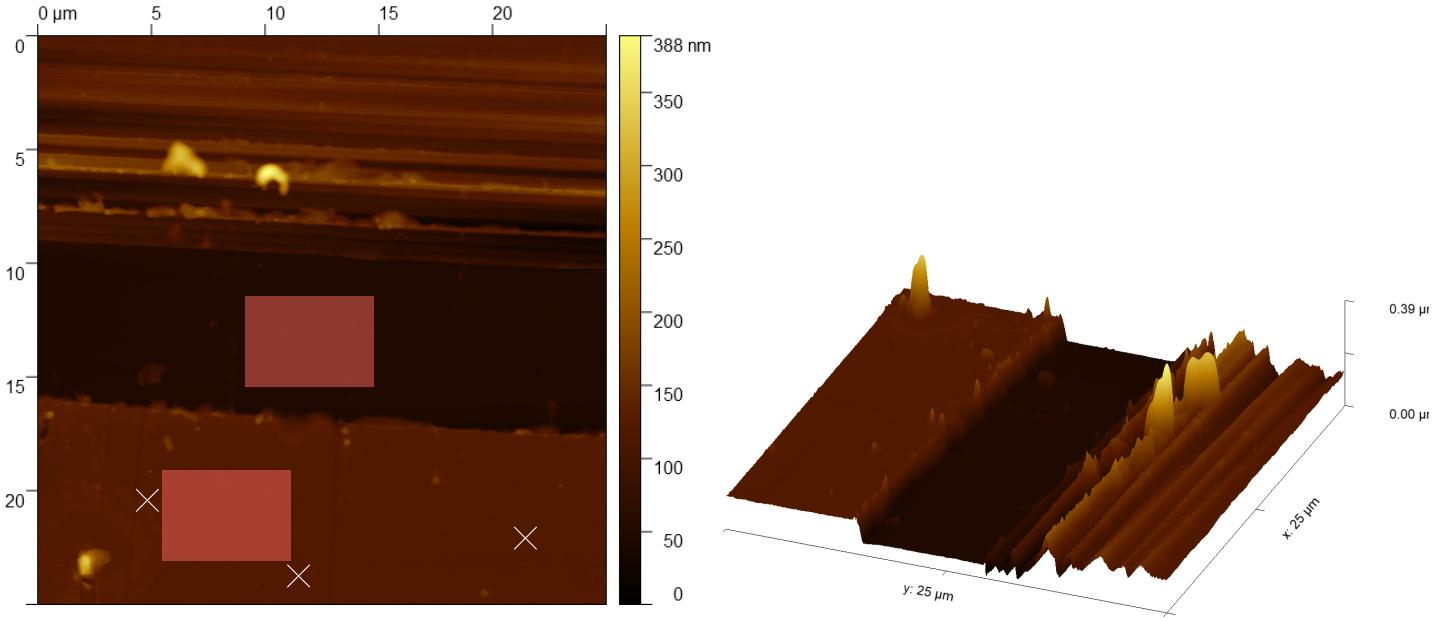

(a) Bottom part of the image, representing the Ag-layer, indicates an exceptional homogeneity of the surface as the color is nearly congruent.

(b) 3D-plot of the surface.

Fig. 8 | AFM-image of the scratched of channel of the Ag-surface after image processing techniques using Gwyddion have been applied.

constant to set the minimum value to zero, ensuring a consistent baseline for further analysis.

5. Tools → Stretch Color Range: This adjustment ensures that the color scale only reaches within the data's actual range, allowing for quick assessment of the height variation represented in the image, while the color map is set to "gold" for improved visualization.

6. Data Process → Basic Operations → Null Offset: This adjustment facilitates information extraction through visual inspection by removing lateral offsets, ensuring both the x- and y-axes start at zero.

The processed height data is presented in Fig. 8a, alongside a 3D visualization in Fig. 8b for enhanced understanding. However, the final portion of our measurement exhibited significant noise for reasons that remain unclear. Importantly, the key part of the data remains unaffected, and our subsequent analysis will focus solely on this crucial segment.

Extracting Dimensions We have now obtained a high resolution image of the channel-like structure of the surface created by the knife. We proceed by extracting ten profile lines along the edge of the channel. Our approach in determining the Ag-layer thickness is to average the z-values over a specified range for both the bottom of the channel as well as the Ag-surface and calculate their separation in z-direction. Lines running perpendicular to the channel were carefully chosen such that they contain as little artifacts as possible. The graphs of the different profile lines are plotted in Fig. 9. A visual examination of the graphs shows no observable evidence of tilt in the data, indicating that our data processing steps were highly effective. Within close vicinity of the edge forming the transition from Ag-surface to channel, large height variations, likely due to material displacement caused from scratching the surface, can be observed. Therefore, we think $0\,\mu\text{m} < x < 3.5\,\mu\text{m}$ and $7.5\,\mu\text{m} < x < 9\,\mu\text{m}$ are reasonable ranges for averaging the plateaus. To better understand the data's roughness within these regions, we extracted their respective minimum and maximum values. A summary of all extracted data is provided in Tab. 2.

surface [nm]			channel [nm]		
$\bar{z}$ (σ)	z_{min}	z_{max}	$\bar{z}$ (σ)	z_{min}	z_{max}
115(2)	112.7	123.3	45.1(7)	43.9	47.4
115(1)	112.0	117.4	45.2(6)	43.8	47.1
116(2)	113.8	125.8	45.4(7)	43.8	47.4
116(1)	113.8	118.1	45.0(6)	44.0	46.6
115.6(9)	113.8	117.4	44.8(5)	43.7	45.9
116(1)	113.1	118.8	44.8(5)	43.9	46.0
115.0(9)	112.9	117.1	44.3(7)	43.1	46.4
116(1)	112.6	118.6	45.3(7)	44.0	46.9
117(1)	115.0	119.7	44.9(7)	43.4	46.9
114.9(7)	113.4	116.2	44.3(5)	43.6	45.4

Tab. 2 | Data from profile line along step.

$\bar{z}_{\text{Ag-surface}} - \bar{z}_{\text{channel}}$	
70(2)	nm
70(1)	nm
71(2)	nm
71(1)	nm
71(1)	nm
71(1)	nm
71(1)	nm
70(1)	nm
73(1)	nm
70.6(8)	nm

Tab. 3 | Ag-layer thickness computed from the individual graphs.

Evaluation and Discussion The separation in z-direction from all the mean values listed in Tab. 2, representing 10 Ag-layer thickness values are provided in Tab 3. Computing the mean gives us:

$$70.8\,\text{nm} \pm 0.2\,\text{nm}$$

It is important to note that our method for determining the Ag-layer thickness introduces a slight bias. This arises because the surface roughness of the Ag layer shifts the overall average slightly in the positive z-direction. To illustrate this effect, we calculate

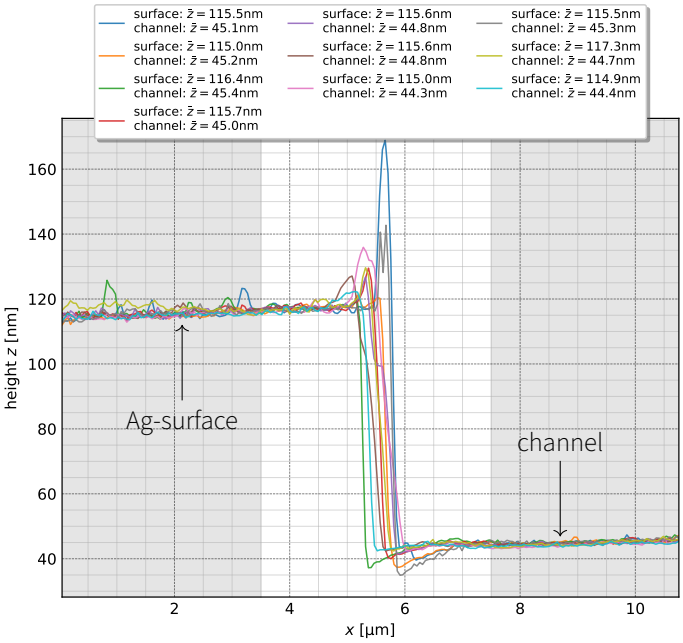

Fig. 9 | Profile line graphs. The ranges in *x*-direction over which have been averaged are indicated in gray.

the variance of the values $z_{\min}$ and $z_{\max}$ for the Ag-surface:

$$\sigma_{\bar{z}_{\min}} = 0.8\,\text{nm}, \quad \sigma_{\bar{z}_{\max}} = 2.9\,\text{nm}$$

In contrast, the variance of these values for the channel is:

$$\sigma_{\bar{z}_{\min}} = 0.3\,\text{nm}, \quad \sigma_{\bar{z}_{\max}} = 0.6\,\text{nm}$$

These values only differ slightly by which the mean value is less affected and therefore the error does not cancel. Further analysis of the RMS roughness values for the areas marked in red in Fig. 8a yielding 1.463 nm (surface) and 0.796 nm (channel) respectively support our assertion. Despite this however, we have successfully determined the Ag-layer thickness with significantly higher precision than our previous profilometer measurement.

REFERENCES

[1] Kateryna Muzyka et al. "DNA at conductive interfaces: What can atomic force microscopy offer?" In: *Journal of Electroanalytical Chemistry* 938 (2023), p. 117448. ISSN: 1572-6657. DOI: https://doi.org/10.1016/j.jelechem.2023.117448. URL: https://www.sciencedirect.com/science/article/pii/S1572665723003089.

[2] Gaoliang Dai, Fan Zhu, and Jens Fluegge. "High-speed metrological large range AFM". In: *Measurement Science and Technology* 26 (July 2015). DOI: 10.1088/0957-0233/26/9/095402.

[3] Chris van Ewijk, Sourav Maity, and Wouter H. Roos. "Visualizing Molecular Dynamics by High-Speed Atomic Force Microscopy". In: *Single Molecule Analysis : Methods and Protocols*. Ed. by Iddo Heller and Erwin J.G. Dulin David nnd Peterman. New York, NY: Springer US, 2024, pp. 355–372. ISBN: 978-1-0716-3377-9. DOI: 10.1007/978-1-0716-3377-9_17. URL: https://doi.org/10.1007/978-1-0716-3377-9_17.

[4] Rafael Daza et al. "Functionalization of atomic force microscopy cantilevers and tips by activated vapour silanization". In: *Applied Surface Science* 484 (2019), pp. 1141–1148. ISSN: 0169-4332. DOI: https://doi.org/10.1016/j.apsusc.2019.04.155. URL: https://www.sciencedirect.com/science/article/pii/S0169433219311535.

[5] Alper D. Ozkan et al. "Probe microscopy methods and applications in imaging of biological materials". In: *Seminars in Cell & Developmental Biology* 73 (2018). Application of Atomic Force Microscopy in cell biology, pp. 153–164. ISSN: 1084-9521. DOI: https://doi.org/10.1016/j.semcdb.2017.08.018. URL: https://www.sciencedirect.com/science/article/pii/S1084952117301921.

[6] Boyu Peng et al. "High performance organic transistor active-matrix driver developed on paper substrate". In: *Scientific reports* 4 (Sept. 2014), p. 6430. DOI: 10.1038/srep06430.

[7] David Nečas and Petr Klapetek. *Gwyddion Documentation*. Nov. 2018. URL: http://gwyddion.net/documentation/ (visited on 11/28/2024).

[8] jpk Instruments. *The NanoWizard AFM Handbook*. 1.3. 2005.

[9] Park Systems. *Standard Imaging Mode – Contact Mode*. Nov. 2024. URL: https://jp.parksystems.com/index.php/jp/park-spm-modes/91-standard-imaging-mode/223-basic-contact-afm-dynamic-force-microscope-dfm (visited on 11/28/2024).

[10] Sebastian Jentsch. *NVIDIA GeForce GT 555M*. May 2018. URL: https://www.notebookcheck.com/NVIDIA-GeForce-GT-555M.41925.0.html (visited on 11/28/2024).

[11] Ahmad Fitri Anuar Mahayudin et al. "Poly-Resistor Thin Film Formation by Excimer Laser Micromachine". In: *Applied Mechanics and Materials* 480 (July 2015), pp. 17–21. DOI: 10.4028/www.scientific.net/AMM.780.17.

[12] Monika Poonia et al. "Development of polycrystalline diffused piezoresistors using e-beam evaporation method for MEMS applications". In: *International Journal of Advancements in Technology; Vol 2, No 1 (2011): International Journal of Advancements in Technology; 108-116* (Jan. 2011).

[13] P Petrik et al. "Comparative study of surface roughness measured on polysilicon using spectroscopic ellipsometry and atomic force microscopy". In: *Thin Solid Films* 315.1 (1998), pp. 186–191. ISSN: 0040-6090. DOI: https://doi.org/10.1016/S0040-6090(97)00349-0. URL: https://www.sciencedirect.com/science/article/pii/S0040609097003490.